

Simulating the formation of massive seed black holes in the early Universe. I: An improved chemical model

Simon C. O. Glover

*Universität Heidelberg, Zentrum für Astronomie, Institut für Theoretische Astrophysik,
Albert-Ueberle-Straße 2, 69120 Heidelberg, Germany*

24 September 2018

ABSTRACT

The direct collapse model for the formation of massive seed black holes in the early Universe attempts to explain the observed number density of supermassive black holes (SMBHs) at $z \sim 6$ by assuming that they grow from seeds with masses $M > 10^4 M_\odot$ that form by the direct collapse of metal-free gas in atomic cooling halos in which H_2 cooling is suppressed by a strong extragalactic radiation field. The viability of this model depends on the strength of the radiation field required to suppress H_2 cooling, J_{crit} : if this is too large, then too few seeds will form to explain the observed number density of SMBHs. In order to determine J_{crit} reliably, we need to be able to accurately model the formation and destruction of H_2 in gas illuminated by an extremely strong radiation field. In this paper, we use a reaction-based reduction technique to analyze the chemistry of H_2 in these conditions, allowing us to identify the key chemical reactions that are responsible for determining the value of J_{crit} . We construct a reduced network of 26 reactions that allows us to determine J_{crit} accurately, and compare it with previous treatments in the literature. We show that previous studies have often omitted one or more important chemical reactions, and that these omissions introduce an uncertainty of up to a factor of three into previous determinations of J_{crit} .

Key words: astrochemistry – hydrodynamics – methods: numerical – molecular processes – cosmology: theory – quasars: general

1 INTRODUCTION

In recent years, infrared sky surveys such as UKIDSS have discovered a number of quasars at redshifts $z > 6$, including the current record holder, a bright quasar at $z = 7.085$ (Mortlock et al. 2011). The presence of these objects indicates that supermassive black holes (SMBHs) with masses of order $10^9 M_\odot$ were already present in the high redshift Universe at a time when the age of the Universe was only ~ 800 million years. However, the existence of these objects is difficult to understand within the standard Λ CDM cosmological model if one assumes that they grew from initial seeds with masses comparable to that of the Sun. Models for accretion onto black holes show that the characteristic growth time for a black hole accreting at the Eddington limit is unlikely to be much smaller than ~ 50 million years, unless one assumes an unreasonably low value for the radiative efficiency of the accretion process. This means that a seed black hole formed at very high redshift can grow by at most a factor of $\sim 10^7$ by the time that the high redshift SMBHs are observed. To produce SMBHs with the observed masses, we therefore require seed black holes with masses $M \sim 100 M_\odot$ or higher

(Tanaka & Haiman 2009). In addition, if one accounts for the fact that radiative and mechanical feedback from the progenitor stars of these seed black holes will remove much of the gas from their local environment, it becomes difficult to see how the required high accretion rates can be sustained at high redshift, further increasing the required seed mass (see e.g. Alvarez, Wise & Abel 2009).

This problem can be avoided if we assume that instead of forming as the remnants of Pop. III stars, the seed black holes that later grow into SMBHs form directly from the monolithic collapse of primordial gas. For this so-called direct collapse model to work, however, it is necessary that the collapsing gas remain warm throughout the collapse, with a temperature of 5000–10000 K (Bromm & Loeb 2003). This keeps the Jeans mass high, preventing the gas from fragmenting into stellar mass clumps, and leading to the formation of a central seed black hole with a mass of order $10^4 M_\odot$ or more (Begelman, Volonteri, & Rees 2006; Choi, Shlosman & Begelman 2013; Latif et al. 2013a). For this model to work, we therefore require a minihalo with a virial temperature in excess of 10^4 K (so that the gas does not simply become thermally supported at low densities) that has not

been enriched with heavy elements, which would otherwise provide efficient cooling down to temperatures $T \ll 10^4$ K (Omukai, Schneider & Haiman 2008). In addition, it is necessary that the formation of H_2 in the gas be strongly suppressed, as otherwise H_2 cooling alone would be sufficient to cool the gas down to temperatures far below 10^4 K (Omukai 2001; Bromm & Loeb 2003). The most viable mechanism known for producing the required suppression of H_2 formation invokes the presence of a very strong extragalactic UV field that immediately photodissociates almost all of the H_2 molecules forming in the gas (Bromm & Loeb 2003; Visbal, Haiman & Bryan 2014), and that also suppresses the formation of H_2 by photodissociating the intermediate H^- and H_2^+ ions (Shang, Bryan & Haiman 2010).

Numerical simulations (see e.g. Bromm & Loeb 2003; Regan & Haehnelt 2009; Shang, Bryan & Haiman 2010; Latif et al. 2013a,b; Becerra et al. 2015; Regan, Johansson, & Haehnelt 2014, as well as the recent reviews by Volonteri 2010, Haiman 2013 and Greif 2015) have confirmed many of the details of this simple model, but have yet to reach agreement regarding the strength of the external radiation field that is required. It is clear that the required radiation field strength is orders of magnitude larger than the mean value produced by early generations of stars (Haiman, Abel & Rees 2000; Greif & Bromm 2006), but it is also clear that the distribution of UV radiation in the early Universe is highly inhomogeneous, owing to the strong clustering of the high-redshift protogalaxies responsible for producing it (Dijkstra et al. 2008; Ahn et al. 2009; Agarwal et al. 2012; Dijkstra et al. 2014). The question of how rarely the required conditions are realized in the early Universe therefore depends sensitively on exactly how strong a UV field is actually required. This is usually quantified in terms of the specific intensity of the radiation field at the Lyman limit. Following Haiman, Abel & Rees (2000), we can measure this in units of $10^{-21} \text{ ergs}^{-1} \text{ cm}^{-2} \text{ Hz}^{-1} \text{ sr}^{-1}$ and write it as J_{21} . The minimum value of J_{21} for which H_2 cooling is sufficiently suppressed is then commonly denoted as J_{crit} .

Values quoted in the literature for J_{crit} range from as low as 20 (Inayoshi & Omukai 2011) to as high as 10^5 (Omukai 2001). Typically, these values are determined by modelling the cooling and collapse of gas within minihalos with $T_{\text{vir}} > 10^4$ K in the presence of a strong UV background using 3D numerical simulations that treat the coupled thermal, chemical and dynamical evolution of the gas. By running the simulation for a range of different values of J_{21} , it is possible to determine the critical value at which H_2 cooling becomes sufficiently suppressed for the direct collapse model to operate.

The scatter in the values of J_{crit} obtained from these studies has several different causes. J_{crit} depends strongly on the spectral shape adopted for the background radiation field (Bromm & Loeb 2003; Shang, Bryan & Haiman 2010) and the manner in which H_2 self-shielding is accounted for (Wolcott-Green & Haiman 2011), and also appears to vary somewhat from minihalo to minihalo (Shang, Bryan & Haiman 2010; Latif et al. 2014). However, an important additional contribution to the uncertainty in J_{crit} comes from the treatment of the gas chemistry within the different studies.

In most cases, the chemical networks used in these studies were originally designed for the study of Pop. III star

formation in the absence of a strong extragalactic radiation field. Although they all include the same basic processes (H_2 formation via the intermediate H^- and H_2^+ ions, H_2 destruction via collisional dissociation, charge transfer with H^+ and photodissociation, and the photodissociation of H^- and H_2^+), the exact set of chemical reactions included varies from network to network. In addition, it is unclear whether *any* of the networks in common usage includes the full set of chemical processes that are important for modelling the formation and destruction of H_2 in an environment much harsher than the one that they were designed to model.

In this paper, we attempt to identify the key reactions that must be accounted for when modelling the chemical evolution of the gas in this environment. To do this, we first model the chemical evolution of the gas using an extensive model of primordial gas chemistry that tracks 30 different chemical species, linked by almost 400 reactions. We then use a reaction-based reduction technique developed by Wiebe, Semenov & Henning (2003) to analyze the chemistry and to identify the main reactions responsible for regulating the H_2 abundance. This allows us to construct a much smaller “reduced” network that contains all of the chemical reactions that must be included in our chemical network if we are to be able to determine J_{crit} accurately.

The plan of the paper is as follows. In Section 2, we present the details of the reaction-based reduction technique and the one-zone chemistry and cooling model used to simulate the thermal and chemical evolution of the gas. In Section 3, we present the results of our analysis and compare our reduced chemical network with other chemical networks used in the literature to simulate the formation of black holes by direct collapse. Finally, we conclude in Section 4 with a brief summary of our main results.

2 NUMERICAL METHOD

2.1 Selecting the set of important reactions

In the direct collapse scenario, the crucial quantity that determines whether or not the gas is able to cool significantly as it undergoes gravitational collapse is the abundance of molecular hydrogen. If the amount of H_2 that forms does not provide sufficient cooling, then the gas remains warm during the collapse, with the temperature T decreasing only slowly as the density increases (see e.g. Omukai 2001; Schleicher, Spaans & Glover 2010). On the other hand, if enough H_2 forms to allow the gas to cool in less than a free-fall time, then the temperature drops dramatically once the density increases above $n \sim 10^2\text{--}10^3 \text{ cm}^{-3}$. To determine the critical Lyman-Werner flux, J_{crit} , one therefore simply needs to find the point at which the strength of the radiation field becomes large enough to suppress the H_2 abundance sufficiently to prevent it from cooling the gas.

It follows from this that in order to determine J_{crit} accurately, we need to have an adequate chemical model of the formation and destruction of H_2 in the gravitationally collapsing gas. At the same time, however, we do not want to make our chemical model larger than is absolutely necessary, as each additional chemical species or chemical reaction that we include will further slow our numerical simulations. We therefore want to identify only those reactions and species

that are most important for modelling the evolution of the H_2 abundance in the collapsing gas.

To do this, we make use of the reaction-based reduction technique developed by Wiebe, Semenov & Henning (2003) and used by them to compute the abundance of carbon monoxide and the fractional ionization of the gas in simulated molecular clouds. The basic idea underlying this technique is quite simple. Starting from a prescribed set of initial conditions, we first compute the chemical and thermal evolution of the gas for a given value of J_{21} using the one-zone model described in Section 2.2 below. The chemical network used in this one-zone model is as extensive as we can reasonably make it, and should therefore include all of the reactions that are likely to play a significant role in the H_2 chemistry.

We next select our starting set of what Wiebe, Semenov & Henning (2003) term “important” species, i.e. those whose abundances we are interested in following accurately. In the present case, this set consists of only a single member – the H_2 molecule – but in principle the same technique can be used with a larger set of important species. We then proceed by determining the dominant production and destruction reactions for each of these species at a set of different output times during the evolution of the gas. If the set of dominant reactions involve chemical species that are not in our starting set, then we add them to the set of important species, and repeat the analysis, proceeding in this fashion until there are no more species or reactions that need to be added. The result is a list of the reactions that are necessary at each output time in order to accurately model the abundances of our starting set of species. The make-up of this list will generally change with time: some reactions that are important at early times will be unimportant at late times, and vice versa. The final set of important reactions can then be obtained simply by combining the individual lists.

To determine the dominant production and destruction reactions at any given output time, we proceed iteratively, as follows. On the first iteration, we set the weights w_s of the important species to 1, and the weights of all other species to 0. We also set the weight of each reaction to zero. We then loop over all of the chemical species included in our chemical model. For each species k , we compute a new weight for each reaction involving that species:

$$w_r^{\text{new}}(j) = \max \left\{ w_r^{\text{curr}}(j), \frac{|R_j|}{\sum_{l=1, N_r(k)} R_l} w_s^{\text{curr}}(k) \right\}. \quad (1)$$

Here, $w_s^{\text{curr}}(k)$ is the current weight of species k , $w_r^{\text{curr}}(j)$ is the current weight of reaction j , $w_r^{\text{new}}(j)$ is the new weight of reaction j , R_j is the rate per unit volume at which reaction j proceeds, and $N_r(k)$ is the number of reactions in which species k participates as either a reactant or a product. Once we have calculated a new weight for every reaction involving species k , we update its weight:

$$w_s^{\text{new}}(k) = \max [w_s^{\text{curr}}(k), \max \{w_r^{\text{new}}(1), \dots, w_r^{\text{new}}(N_r(k))\}]. \quad (2)$$

In other words, we take the new species weight to be the largest value from amongst the weights of the reactions involving that species, unless this is smaller than the current weight of the species. Having determined new weights for every species, we begin a new iteration, using the updated weights in Equation 1 above. We continue to iterate until

all of the species weights have converged to within some pre-specified tolerance.

One situation in which this procedure can give misleading results occurs when the formation and destruction of one of the species is dominated by a single forwards reaction and its inverse. Consider, for example, the case of the formation of HD from H_2



In warm gas, this reaction occurs very rapidly, but so does its inverse



In the extreme case in which these reactions are perfectly balanced, both can have large R values, and hence potentially also large weights, and yet the net effect of the pair of reactions is to leave the abundances of all of the species involved unchanged. In our analysis, we attempt to mitigate the impact of this problem by identifying reaction pairs of this kind and replacing the reaction rates used for these reactions in Equation 1 with the absolute value of the difference between the forward and reverse reaction rates; in the example above, this corresponds to the net rate at which H_2 is formed or destroyed by the pair of reactions.

Our analysis procedure leaves us with a list of weights for every reaction that is valid for the output time considered. We can convert this into a list of reactions by retaining only those reactions whose weights exceed some cut-off value ϵ . As we show later in Section 3.3, setting $\epsilon = 10^{-4}$ enables us to generate a subset of reactions that allow us to determine J_{crit} to within an accuracy of around 1% when compared to the results of models run with the full chemical network.

By repeating the same procedure for many different output times, and combining the individual reaction lists, we can construct a reduced reaction network that is sufficient for modelling the chemical evolution of H_2 over the entire period simulated in our one-zone model. In principle, the reduced reaction network that we derive in this fashion is specific to our choice of J_{21} and to the initial conditions for our simulation. However, by re-running the one-zone model and repeating the same analysis procedure for many different values of J_{21} with various different sets of initial conditions, as described in Section 2.2 below, and the combining the resulting reduced networks, we can arrive at a final reduced network that is valid over the whole range of physical conditions that are of interest to us.

2.2 The one-zone model

2.2.1 Basic details

In order to model the chemical and thermal evolution of gravitationally-collapsing primordial gas illuminated by a strong extragalactic radiation field, we use a simple one-zone model that is derived from the one presented in Glover & Savin (2009). The gas density is assumed to evolve as

$$\frac{d\rho}{dt} = \frac{\rho}{t_{\text{ff}}}, \quad (5)$$

where $t_{\text{ff}} = (3\pi/32G\rho)^{1/2}$ is the free-fall time of the gas. To follow the thermal evolution of the gas, we write the internal energy equation as

$$\frac{de}{dt} = \frac{p}{\rho^2} \frac{d\rho}{dt} + \Gamma - \Lambda, \quad (6)$$

where e is the internal energy density, $p = (\gamma - 1)e$ is the gas pressure, Γ is the radiative and chemical heating rate per unit volume and Λ is the radiative and chemical cooling rate per unit volume.

We compute Γ and Λ using a detailed atomic and molecular cooling function based on the one presented in Section 4 of Glover & Savin (2009). In an effort to use the most up-to-date atomic and molecular data available, we have updated two of the cooling processes included in the model: the collisional excitation of H_2 by collisions with protons and by collisions with electrons. Full details of these updates are given in Appendix A.

To model the chemical evolution of the gas, we use a modified version of the chemical network present in Glover & Savin (2009). The original version of this network tracked the abundance of 30 different primordial chemical species and included a total of 392 reactions. We have extended this model by including three new reactions not treated in Glover & Savin (2009): the collisional ionization of atomic hydrogen by collisions with H or He, and the collisional dissociation of H_2^+ by H. Details of these new reactions are given in Appendix B. We have also updated several of the reaction rates in light of new theoretical or experimental data. Again, full details of these modifications are given in Appendix B.

2.2.2 Photochemistry and self-shielding

The rate coefficients listed in Glover & Savin (2009) for the various photochemical reactions assumed that the external background radiation field had the spectral shape of a 10^5 K black-body, cut-off at energies of 13.6 eV and above to account for the effects of absorption by atomic hydrogen in the intergalactic medium. This choice of spectrum (which we refer to hereafter as a T5 spectrum, for brevity) was motivated by the fact that we expect the brightest Pop. III stars to have effective temperatures of around this value (see e.g. Cojazzi et al. 2000). However, this is a reasonable approximation only when the dominant contribution to the extragalactic background radiation field does indeed come from very massive Pop. III stars, specifically those with masses greater than around $100 M_\odot$ (Bromm, Kudritzki, & Loeb 2001). If a significant fraction of the radiation comes instead from less massive Pop. III stars or from Pop. II stars with systematically lower effective temperatures, then the ratio of the UV to the optical flux can potentially be much smaller than with a T5 spectrum, with important implications for the relative importance of H_2 photodissociation and H^- photodetachment. Several authors have attempted to quantify the dependence of J_{crit} on the spectral shape of the extragalactic radiation field by performing simulations both with a T5 spectrum and with a T4 spectrum: a 10^4 K diluted black-body with a similar high-energy cut-off to the T5 spectrum. These studies (see e.g. Bromm & Loeb 2003; Shang, Bryan & Haiman 2010) find that the choice of spectrum has a large influence on the value of J_{crit} . For instance, Shang, Bryan & Haiman (2010) find that in their models, the value

of J_{crit} for a T5 spectrum lies in the range $10^4 < J_{\text{crit}} < 10^5$, but that for a T4 spectrum, $30 < J_{\text{crit}} < 300$, a difference of two orders of magnitude or more.

To account for this uncertainty, we perform two sets of simulations: one set using a T5 spectrum and a second set using a T4 spectrum. For the runs with the T5 spectrum, we use the photochemical rates listed in Glover & Savin (2009) for all processes except for the photodissociation of H_2^+ , which is treated with the density-dependent approach described in Appendix B2. For the other set of runs, we have recomputed the photochemical rates using a T4 spectrum and the same basic approach as in Glover & Savin (2009).

In practice, of course, both the T4 and T5 spectra are relatively crude approximations to the actual spectrum of the extragalactic background produced by high-redshift star-forming protogalaxies (Agarwal & Khochfar 2015; Sugimura, Omukai & Inoue 2014; Latif et al. 2015). However, they should bracket the behaviour seen in more realistic models, making them suitable choices for the purposes of our study.

When treating most of the photochemical reactions, we assume that the gas remains optically thin, as the continuum opacity of low density primordial gas is very small (see e.g. Lenzuni, Chernoff & Salpeter 1991). The important exception is H_2 photodissociation, as the rate of this processes can be strongly affected by H_2 self-shielding. To account for this, we use the modified form of the Draine & Bertoldi (1996) shielding function introduced by Wolcott-Green, Haiman & Bryan (2011):

$$f_{\text{sh}}(N_{\text{H}_2}, T) = \frac{0.965}{(1 + x/b_5)^{1.1}} + \frac{0.035}{(1 + x)^{0.5}} \times \exp[-8.5 \times 10^{-4}(1 + x)^{0.5}], \quad (7)$$

where $x = N_{\text{H}_2}/5 \times 10^{14} \text{ cm}^{-2}$, $b_5 = b/10^5 \text{ cm s}^{-1}$, and b is the Doppler broadening parameter, which we assume to be dominated by the effects of thermal broadening. In order to evaluate this expression for f_{sh} , we need to know the column density of H_2 in the collapsing gas cloud. We compute this using a similar method to Omukai (2001): we assume that the dominant contribution to the shielding comes from a core region with radius $R_c = \lambda_J$, where λ_J is the Jeans length. The required H_2 column density then follows as $N_{\text{H}_2} = n_{\text{H}_2} R_c = n_{\text{H}_2} \lambda_J$, where n_{H_2} is the number density of H_2 in our one-zone model.

It should be noted that the simple approximation that we use here to compute N_{H_2} has been shown to overestimate the actual amount of shielding by up to an order of magnitude in some cases compared to the results of fully 3D treatments (Wolcott-Green, Haiman & Bryan 2011). For this reason, the absolute values of J_{crit} that we derive in this study should be treated with considerable caution. However, this simplification should not affect our conclusions regarding the set of chemical reactions that are required to accurately determine J_{crit} , or our findings regarding the sensitivity of J_{crit} to uncertainties in the rates of these reactions.

2.2.3 Initial conditions

We perform simulations using three different set of initial conditions, as detailed in Table 1. In runs 1 and 4, we start with a low initial temperature, $T_0 = 200$ K, and an initial

Table 1. List of simulations

Run	T_0 (K)	$x_{e,0}$	$x_{H_2,0}$	Spectrum
1	200	2×10^{-4}	2×10^{-6}	T4
2	8000	2×10^{-4}	2×10^{-6}	T4
3	8000	1.0	0.0	T4
4	200	2×10^{-4}	2×10^{-6}	T5
5	8000	2×10^{-4}	2×10^{-6}	T5
6	8000	1.0	0.0	T5

fractional ionization and H_2 fractional abundance close to those found in the IGM prior to the onset of Pop. III star formation ($x_{e,0} = 2 \times 10^{-4}$, $x_{H_2,0} = 2 \times 10^{-6}$). In runs 2 and 5, we start with the same chemical composition but with a much higher gas temperature, $T_0 = 8000$ K. Finally, in runs 3 and 6, we set $T_0 = 8000$ K, but assume that the gas was initially fully ionized ($x_{e,0} = 1.0$, $x_{H_2,0} = 0.0$). The initial density in all of the simulations is set to $n_0 = 0.3 \text{ cm}^{-3}$, corresponding approximately to the mean density within the virial radius of a protogalaxy forming at a redshift $z = 20$. We have explored the effects of adopting a larger initial density but find that this makes little difference to our results.

In all of our simulations, we adopt an elemental abundance (relative to hydrogen) of $A_D = 2.6 \times 10^{-5}$ for deuterium and $A_{Li} = 4.3 \times 10^{-10}$ for lithium (Cyburt 2004). We set the initial abundances of D^+ and HD so that they are a factor of A_D smaller than the initial H^+ and H_2 abundances, respectively. We assume that the lithium was initially entirely in neutral atomic form, and set the initial abundances of all of the other chemical species to zero.

For each set of initial conditions, we run two different sets of simulations, one with a T4 spectrum and the other with a T5 spectrum, as indicated in Table 1.

3 CONSTRUCTION OF AN ACCURATE REDUCED NETWORK

3.1 Determination of J_{crit}

Before we can identify the set of reactions that it is necessary to include in the chemical model in order to accurately determine J_{crit} , it is first necessary to establish the value of J_{crit} for each of our six different setups. We do this using a binary search method. We start by selecting two values of J_{21} that are certain to bound J_{crit} : a low value, $J_{21,\text{low}} = 1$, that we have verified is too small to prevent efficient H_2 cooling from occurring in any of the models, and a high value, $J_{21,\text{high}} = 10^4$, that completely suppresses H_2 cooling in all of the models. We then compute a new value of J_{21} using the equation

$$J_{21,\text{new}} = (J_{21,\text{low}} \times J_{21,\text{high}})^{1/2}, \quad (8)$$

and run a simulation using this new value. If $J_{21,\text{new}}$ is large enough to prevent efficient H_2 cooling, then we adopt it as our new value of $J_{21,\text{high}}$; otherwise, we take it as our new value of $J_{21,\text{low}}$. We proceed in this fashion until the difference between $J_{21,\text{low}}$ and $J_{21,\text{high}}$ is less than 0.2%, and take the final value of $J_{21,\text{new}}$ as our estimate for J_{crit} . The resulting values are listed in Table 2 for each of our six different setups. In agreement with previous work, we find that the choice of spectral shape has a large influence on J_{crit} .

Table 2. Critical Lyman-Werner flux as a function of ϵ

Run	J_{crit}				
	$\epsilon = 0$	$\epsilon = 10^{-4}$	$\epsilon = 10^{-3}$	$\epsilon = 0.01$	$\epsilon = 0.1$
1	17.0	17.1	17.1	17.1	17.5
2	18.0	18.0	18.0	18.1	18.6
3	18.0	18.1	18.1	18.1	18.6
4	1640	1640	1640	1650	4260
5	1630	1630	1630	1640	4260
6	1630	1630	1630	1640	4260

The values shown here are specified to only three significant figures, and were computed using chemical networks consisting of all chemical reactions with maximum weights exceeding the listed value of ϵ . The case $\epsilon = 0$ corresponds to the full chemical model.

With a T4 spectrum, we find that $J_{\text{crit}} \sim 17$ –18, while a T5 spectrum yields $J_{\text{crit}} \sim 1630$. We see also that the results that we obtain are not particularly sensitive to our choice of initial conditions.

It is interesting to compare our results to those of previous one-zone studies. For the T4 spectrum, our finding that $J_{\text{crit}} \sim 17$ –18 is in fairly good agreement with the values $J_{\text{crit}} = 20, 25, 39$ derived by Inayoshi & Omukai (2011), Sugimura, Omukai & Inoue (2014), and Shang, Bryan & Haiman (2010), respectively. The difference between our value and the values derived in these other studies is most likely due to the impact of the differences in the chemical model and the choices made for some of the key rate coefficients, since as we will see later in this paper and in Paper II (Glover 2015), these differences can easily introduce an uncertainty of a factor of a few into our estimates for J_{crit} .

For the T5 spectrum, our value of J_{crit} is almost an order of magnitude smaller than the values of $J_{\text{crit}} = 1.2 \times 10^4$ and 1.6×10^4 found by Shang, Bryan & Haiman (2010) and Inayoshi & Omukai (2011), respectively. However, this difference can be explained by differences in our treatment of H_2 self-shielding. Both of these previous studies used the H_2 self-shielding function computed by Draine & Bertoldi (1996), while we used instead the modified version given in Wolcott-Green, Haiman & Bryan (2011), which more accurately treats the self-shielding of H_2 in hot gas. Sugimura, Omukai & Inoue (2014) performed one-zone calculations with a T5 spectrum using both of these treatments of H_2 self-shielding, and showed that the value of J_{crit} that they obtained with the Wolcott-Green, Haiman & Bryan (2011) treatment was approximately an order of magnitude smaller than that obtained using the Draine & Bertoldi (1996) treatment. The value they obtained for J_{crit} with the Wolcott-Green, Haiman & Bryan (2011) treatment was $J_{\text{crit}} \simeq 1400$, in good agreement with the value we find using our model.

3.2 The reduced network

Having determined the value of J_{crit} in each run, we next analyze the full set of chemical reactions taking place during the evolution of the gas, as outlined in Section 2.1. For each run, we consider a large set of output times, and use our computed values for the density, temperature and chemical composition of the gas to determine the weight of each reaction in our full set at that output time. We record these

weights, and repeat this procedure for a large number of different output times. We then determine the maximum weight for each reaction in our model. To help ensure that our reduced network will be robust against minor changes in the physical conditions in the gas, we consider not only the case when $J_{21} = J_{\text{crit}}$, but also perform the same analysis for simulations with $J_{21} = 0.3J_{\text{crit}}$ and $J_{21} = 3J_{\text{crit}}$, taking the maximum weight for each reaction to be the largest of the weights obtained for the reaction with these three different setups. Finally, we construct our reduced network using only those reactions whose maximum weights exceed $\epsilon = 10^{-4}$. The resulting set of reactions for each run is listed in Table 3, along with the corresponding set of maximum weights.

We see immediately that there is a subset of reactions with very large weights that appear in the reduced network for each of our runs. This is not surprising: most of the reactions in this set play such important roles in the regulation of the H_2 abundance that any model omitting them could not hope to be representative of the real behaviour of the gas. Examples include the photodissociation and collisional dissociation of H_2 , the formation of H_2 from H^- , or the formation and photodissociation of the H^- ion itself.

There are also a few reactions that have relatively high weights in some of our runs that are more unexpected. Perhaps the best example of these is the collisional ionization of atomic hydrogen by collisions with other hydrogen atoms, i.e.



Most previous networks developed to treat primordial chemistry have omitted this reaction¹, assuming it to be unimportant in comparison to the collisional ionization of hydrogen by electrons, since the latter reaction has a far larger rate coefficient. However, while it is certainly true that collisions with electrons dominate in many circumstances – for example in gas cooling and recombining from an initially ionized state – this is not true in all of the runs we examine here. In particular, if the initial electron abundance is small, as for example in runs 1 or 2, then collisions between hydrogen atoms happen so much more frequently than collisions between hydrogen atoms and electrons that this reaction can come to dominate the ionization rate despite its small rate coefficient.

To illustrate the importance of this reaction, we re-ran our determination of J_{crit} for models 1 and 4 with the value of its rate coefficient set to zero. We found that in this case $J_{\text{crit}} = 11.8$ for run 1 and $J_{\text{crit}} = 1280$ for run 4. In other words, omitting this reaction leads to a 20–30% decrease in the derived value of J_{crit} when we start from low ionization initial conditions. If we also disable the reaction



which again is often omitted from treatments of primordial chemistry, then J_{crit} is reduced even further, to $J_{\text{crit}} = 8.9$ or 1110 for runs 1 and 4, respectively.

¹ The notable exception is Omukai (2001), who does include this process in his chemical network. Studies of SMBH formation that make use of his network (e.g. Sugimura, Omukai & Inoue 2014) therefore already account for this reaction.

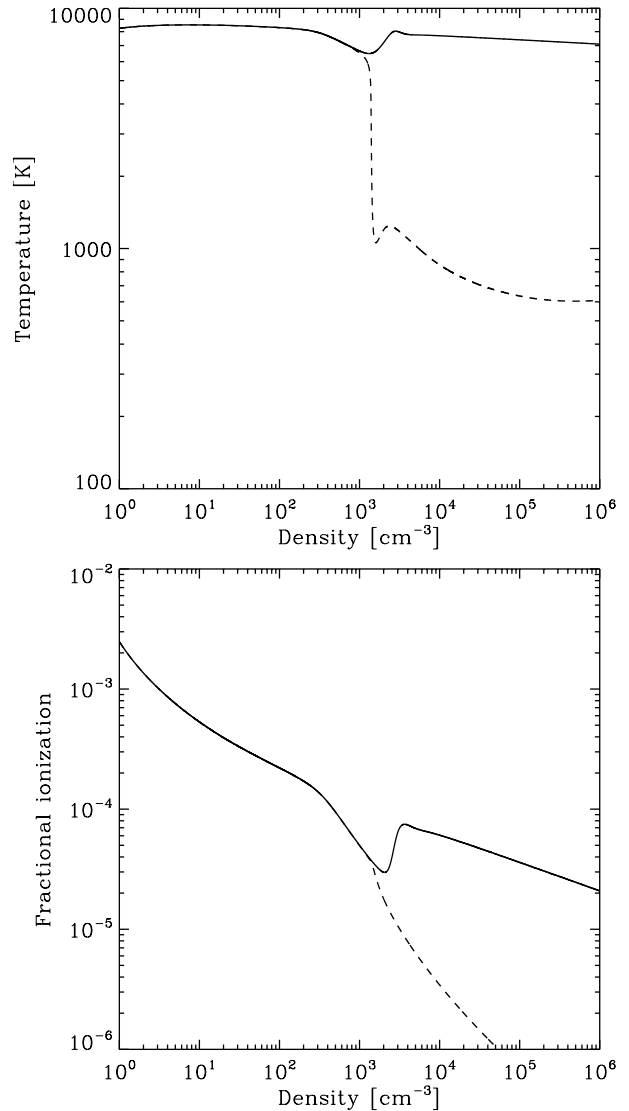


Figure 1. *Top panel:* evolution of the gas temperature as a function of the hydrogen nuclei number density in runs with the same setup as in run 6 (a T5 spectrum, fully ionized initial conditions). Results are shown for $J_{21} = 1630$ (solid line) and $J_{21} = 1635$ (dashed line). *Bottom panel:* evolution of the fractional ionization as a function of density in the same runs.

We can understand why these two reactions appear to be so important for determining J_{crit} if we examine how the fractional ionization of the gas evolves as a function of density when J_{21} is close to J_{crit} . In Figure 1, we show how the temperature and the fractional ionization evolve with density in two simulations carried out with the same initial conditions as run 6 (i.e. fully ionized gas, illuminated by a T5 spectrum), with $J_{21} = 1630$ (dashed line) and $J_{21} = 1635$ (solid line). These two values of J_{21} were chosen to tightly bracket J_{crit} . We see that in both simulations, the temperature evolution is essentially identical until we reach a density of $n \sim 10^3 \text{ cm}^{-3}$. At this point, the behaviour of the two runs diverges. In the run with $J_{21} < J_{\text{crit}}$, the H_2 fraction in the gas at this point is high enough to allow it to begin to cool significantly. As it cools, the effects of H_2 collisional dissociation become less effective, allowing the H_2

Table 3. List of reactions with maximum reaction weights greater than 10^{-4} in at least one simulation

No.	Reaction	Maximum reaction weight					
		Run 1	Run 2	Run 3	Run 4	Run 5	Run 6
1	$\text{H}_2 + \gamma \rightarrow \text{H} + \text{H}$	1.00	1.00	1.00	1.00	1.00	1.00
2	$\text{H}_2 + \text{H} \rightarrow \text{H} + \text{H} + \text{H}$	0.49	0.50	0.49	0.49	0.49	0.49
3	$\text{H}^- + \text{H} \rightarrow \text{H}_2 + \text{e}^-$	0.47	0.47	0.47	0.50	0.47	0.47
4	$\text{H}_2^+ + \text{H} \rightarrow \text{H}_2 + \text{H}^+$	0.41	0.49	0.48	4.7×10^{-2}	4.3×10^{-2}	4.4×10^{-2}
5	$\text{H}^+ + \text{e}^- \rightarrow \text{H} + \gamma$	0.27	0.12	0.48	4.7×10^{-3}	1.0×10^{-2}	4.3×10^{-2}
6	$\text{H} + \text{e}^- \rightarrow \text{H}^- + \gamma$	0.23	0.23	0.23	0.25	0.23	0.24
7	$\text{H}^- + \gamma \rightarrow \text{H} + \text{e}^-$	0.21	0.15	0.14	0.25	0.23	0.23
8	$\text{H} + \text{H}^+ \rightarrow \text{H}_2^+ + \gamma$	0.20	0.24	0.24	2.3×10^{-2}	2.2×10^{-2}	2.1×10^{-2}
9	$\text{H}_2^+ + \gamma \rightarrow \text{H}^+ + \text{H}$	0.12	0.24	0.24	7.2×10^{-3}	2.1×10^{-2}	2.0×10^{-2}
10	$\text{H} + \text{H} \rightarrow \text{H}^+ + \text{e}^- + \text{H}$	9.5×10^{-2}	0.12	1.1×10^{-2}	1.4×10^{-2}	1.1×10^{-2}	1.4×10^{-3}
11	$\text{H}^- + \text{H} \rightarrow \text{H} + \text{H} + \text{e}^-$	8.8×10^{-2}	8.9×10^{-2}	8.8×10^{-2}	9.3×10^{-2}	9.2×10^{-2}	9.2×10^{-2}
12	$\text{H} + \text{e}^- \rightarrow \text{H}^+ + \text{e}^- + \text{e}^-$	6.1×10^{-2}	0.22	4.0×10^{-2}	7.8×10^{-3}	2.0×10^{-2}	3.9×10^{-3}
13	$\text{H}_2^+ + \text{He} \rightarrow \text{HeH}^+ + \text{H}$	3.5×10^{-2}	2.8×10^{-3}	2.7×10^{-3}	3.6×10^{-4}	3.0×10^{-4}	3.0×10^{-4}
14	$\text{H} + \text{He} \rightarrow \text{H}^+ + \text{e}^- + \text{He}$	2.7×10^{-2}	3.6×10^{-2}	3.1×10^{-3}	3.3×10^{-3}	3.2×10^{-3}	3.9×10^{-4}
15	$\text{H}_2 + \text{H}^+ \rightarrow \text{H}_2^+ + \text{H}$	1.0×10^{-2}	8.0×10^{-3}	4.2×10^{-2}	1.1×10^{-3}	1.1×10^{-3}	1.1×10^{-3}
16	$\text{H}_2 + \text{He} \rightarrow \text{H} + \text{H} + \text{He}$	5.9×10^{-3}	5.9×10^{-3}	5.9×10^{-3}	5.8×10^{-3}	5.8×10^{-3}	5.8×10^{-3}
17	$\text{HeH}^+ + \text{H} \rightarrow \text{H}_2^+ + \text{He}$	2.3×10^{-3}	2.8×10^{-3}	2.6×10^{-3}	3.6×10^{-4}	3.0×10^{-4}	3.0×10^{-4}
18	$\text{H} + \text{H} + \text{H} \rightarrow \text{H}_2 + \text{H}$	1.4×10^{-3}	1.3×10^{-3}	1.3×10^{-3}	—	—	—
19	$\text{H}^- + \text{He} \rightarrow \text{H} + \text{He} + \text{e}^-$	1.3×10^{-3}	1.4×10^{-3}	1.3×10^{-3}	2.5×10^{-3}	2.0×10^{-3}	1.9×10^{-3}
20	$\text{H}_2^+ + \text{H} \rightarrow \text{H} + \text{H}^+ + \text{H}$	1.3×10^{-3}	3.6×10^{-4}	5.2×10^{-4}	—	—	—
21	$\text{He} + \text{H}^+ \rightarrow \text{HeH}^+ + \gamma$	5.3×10^{-4}	—	—	—	—	—
22	$\text{H}^- + \text{H}^+ \rightarrow \text{H} + \text{H}$	4.6×10^{-4}	4.6×10^{-4}	4.0×10^{-4}	7.5×10^{-4}	1.4×10^{-3}	6.6×10^{-2}
23	$\text{H}_2^+ + \text{e}^- \rightarrow \text{H} + \text{H}$	1.7×10^{-4}	2.0×10^{-4}	2.4×10^{-2}	—	—	8.7×10^{-4}
24	$\text{HeH}^+ + \text{e}^- \rightarrow \text{He} + \text{H}$	—	—	1.9×10^{-4}	—	—	—
25	$\text{H}^- + \text{H}^+ \rightarrow \text{H}_2^+ + \text{e}^-$	—	—	1.0×10^{-4}	—	—	9.6×10^{-4}
26	$\text{H}^- + \text{e}^- \rightarrow \text{H} + \text{e}^- + \text{e}^-$	—	—	—	1.0×10^{-4}	2.6×10^{-4}	9.5×10^{-3}

The reactions with numbers listed in bold font make up the minimal reduced model described in Section 3.3.

fraction to increase further, and so the cooling runs away, rapidly driving the temperature down to $T \sim 1000$ K. In the run with $J_{21} > J_{\text{crit}}$, on the other hand, the smaller H_2 abundance means that H_2 cooling never becomes effective and the gas remains hot throughout the simulation.

The value of J_{crit} is therefore determined in this case by the chemical state of the gas at $n \sim 10^3 \text{ cm}^{-3}$ and $T \sim 7500$ K. The H_2 fraction in the gas in these conditions depends on the fractional ionization. Figure 1 shows that even though the gas is initially fully ionized, by the time we reach $n \sim 10^3 \text{ cm}^{-3}$, the fractional ionization has lost its memory of this initial state and has decreased to $x \sim 4 \times 10^{-5}$. This value is set by the balance between the collisional ionization of hydrogen by collisions with electrons, H atoms and He atoms (i.e. reactions 12, 10, and 14, respectively) and the radiative recombination of H^+ . If we compare the rates of reactions 10, 12 and 14 in these conditions, we find that $R_{10} \simeq 4 \times 10^{-16} \text{ cm}^{-3} \text{ s}^{-1}$, $R_{12} \simeq 2 \times 10^{-16} \text{ cm}^{-3} \text{ s}^{-1}$ and $R_{14} \simeq 10^{-16} \text{ cm}^{-3} \text{ s}^{-1}$. In other words, because of the very low fractional ionization of the gas, reactions 10 and 14 between them provide around 70% of the total collisional ionization rate, with the main contribution coming from reaction 10. Omitting these reactions therefore leads to a factor of ~ 3 error in the total ionization rate, and hence a factor of ~ 2 error in the fractional ionization. This reduces the H_2 formation rate by a similar amount and hence also reduces our estimate of J_{crit} .

Another interesting thing that Table 3 shows us is that once we start to look at reactions with lower weights, which are less important overall for our determination of J_{crit} , we

see substantially more variation from run to run. Only for runs 4 and 5 does our reaction weighting algorithm provide us with exactly the same set of reactions with maximum weights greater than ϵ ; for the other runs, we see minor differences, generally involving a small number of processes with weights close to our cut-off. In order to have a reaction network that is robust to changes in the initial conditions and details of the background radiation field, we therefore recommend that one uses all of the 26 reactions listed in Table 3.

3.3 Effect of varying ϵ

In order to establish that our choice of a value of $\epsilon = 10^{-4}$ for the reaction weight cut-off in our selection algorithm does indeed allow us to select all of the reactions important for determining J_{crit} , we re-ran our models using a reduced chemical network consisting only of the 26 reactions listed in Table 3 and recalculated J_{crit} for each model using the same approach as before. The resulting values are shown in Table 2. We see that there are minor differences in the predicted values of J_{crit} in a couple of the runs, but that they are at the level of less than 1%. This is much smaller than the scatter in J_{crit} from halo to halo caused by differences in the dynamical evolution of the gas (Latif et al. 2014). This demonstrates that our 26 reaction reduced network is indeed accurate enough for our purposes.

The question then naturally arises as to whether we can simplify our reduced network even more. If we increase the value of ϵ , and hence select even fewer reactions to join the

set of “important” reactions, then how badly does this compromise our ability to determine J_{crit} accurately? To explore this, we constructed several additional reduced networks, in which we retained only those reactions with maximum weights greater than $\epsilon = 10^{-3}$, 0.01 or 0.1 in at least one run, and then used these even more highly simplified networks to determine J_{crit} . When performing this analysis for the $\epsilon = 0.01$ case, we found that in order to produce meaningful results, it was necessary to include one reaction – the destruction of HeH^+ by collisions with H, reaction 17 in the Table – that formally has a weight that is less than 0.01. The reason for this is that otherwise our $\epsilon = 0.01$ model would contain a reaction that forms HeH^+ (reaction 13 in the Table), but no reaction that destroys it, meaning that the abundance of HeH^+ would increase indefinitely.

The results that we obtained when varying ϵ are shown in columns 4-6 of Table 2. We see that the results we obtain for $\epsilon = 10^{-3}$ or $\epsilon = 0.01$ are very similar to those we obtain in the $\epsilon = 10^{-4}$ case, with the derived values of J_{crit} differing by no more than around 1%. However, in the $\epsilon = 0.1$ case, we see a clear change in behaviour: the error in the value of J_{crit} we obtain for the T5 spectrum has increased from $\sim 1\%$ to a factor of a few. This suggests that if we want to simplify the chemistry as much as possible while still being able to determine J_{crit} accurately, then the best choice is a minimal reduced network consisting of reactions 1–15, 17, 22, and 23. On the other hand, if we want to be a little more conservative, in view of the fact that the physical conditions encountered in more realistic simulations are not perfectly reproduced by our one-zone model, then we should retain all 26 of the reactions listed in Table 3.

3.4 Sensitivity to the treatment of H_2^+ excitation

As we discuss in more detail in the Appendix, the rate at which H_2^+ is destroyed by processes such as dissociative recombination or photodissociation is highly sensitive to the vibrational state of the molecular ions: it is far easier to destroy H_2^+ ions in states with $v \gg 0$ than ones that are in the $v = 0$ vibrational ground state. Therefore, any model of the chemistry of H_2^+ in primordial gas should also account, at least approximately, for the degree of excitation of the ions. In the chemical model presented in this paper, this is done in a simple but approximate fashion, for reasons of computational convenience. However, in principle one can construct far more complex and accurate models (see e.g. Coppola et al. 2011). An obvious question is therefore whether this complexity is necessary if one wants to accurately determine J_{crit} , or whether the simple treatment used in this paper suffices.

To answer this question, we performed two additional sets of runs. In the first set, we artificially set the H_2^+ critical density to a very large number, so that all of the chemical rates used for the ion were the ones for H_2^+ in its ground state. In the second set of runs, we instead set the H_2^+ critical density to zero, so that the local thermodynamic equilibrium (LTE) rates were used for all of the reactions involving H_2^+ as a reactant. These two limiting cases should bracket the real behaviour of the H_2^+ ions in the gas, and so by comparing the results of these two sets of runs, we can establish how sensitive J_{crit} is to the details of the excitation of the H_2^+ ions.

Table 4. Dependence of J_{crit} on our treatment of H_2^+ excitation

Run	Fiducial	J_{crit}	
		$v = 0$	LTE
1	17.0	17.6	14.2
2	18.0	18.6	14.5
3	18.0	18.6	14.5
4	1640	1650	1560
5	1630	1640	1560
6	1630	1640	1560

We show the results from these two sets of runs in Table 4, along with the results from our fiducial model for comparison. We see that there is only a small difference between the values of J_{crit} that we obtain using our fiducial model and those from the $v = 0$ model. This is not surprising, since the question of whether or not enough H_2 forms to cool the gas is largely determined by the chemistry occurring at densities $n < n_{\text{crit}}$, where the $v = 0$ rates are a good approximation. If we instead adopt LTE rates throughout, we find a larger difference between the models, approximately 20% in the runs with the T4 spectrum and $\sim 5\%$ in the runs with the T5 spectrum. As this represents a worst case, the real error introduced is almost certainly smaller than this. Our simplified treatment of H_2^+ excitation therefore does not represent a major source of error in our determination of J_{crit} .

3.5 Importance of dissociative tunneling

Our analysis in Section 3.2 showed that the collisional dissociation of H_2 has one of the largest weights in our reduced chemical network, and therefore it is very important to treat this process accurately. As discussed at some length in e.g. Martin, Schwarz & Mandy (1996), there are two distinct processes that contribute to the total collisional dissociation rate. The first is direct collisional dissociation, where the H_2 molecule undergoes a transition from a bound state directly into the continuum of classically unbound states. The second is dissociative tunneling, where the H_2 molecule is excited into a quasi-bound state – a state that has an internal energy larger than is required for dissociation, but which is separated from the continuum by a barrier in the effective potential. Quantum tunneling through this barrier then leads to spontaneous dissociation. In low density gas this process of dissociative tunneling can make a major contribution to the total collisional dissociation rate.

Some studies of the direct collapse model for the formation of massive black holes include only the effects of direct collisional dissociation, and not those of dissociative tunneling (e.g. Shang, Bryan & Haiman 2010), but as Latif et al. (2014) point out, this potentially introduces significant uncertainty into the resulting values derived for J_{crit} . In an effort to quantify this uncertainty, we re-ran our set of six simulations using our reduced chemical model, but with the effects of dissociative tunneling disabled. We found that in this case, $J_{\text{crit}} = 33.1$ in runs 1–3 and $J_{\text{crit}} = 2780$ in runs 4–6. In other words, the failure to account for this process when modelling H_2 dissociation in this scenario can introduce an error of almost a factor of two into J_{crit} .

Table 5. Comparison of J_{crit} determined using our reduced model with that determined using several other simplified models from the literature

Run	This work	J_{crit}		Omukai (2001)
		KROME	ENZO	
1	17.1	8.9	21.5	17.1
2	18.0	14.7	26.7	18.3
3	18.1	14.9	26.8	18.3
4	1640	1120	1930	3040
5	1630	1160	1940	3040
6	1630	1160	1940	3040

3.6 Comparison with other chemical models

It is interesting to investigate whether there are any significant differences between the reduced chemical network constructed in this paper and the other chemical networks in common usage in studies of the direct collapse model for the formation of massive black holes. The majority of existing studies use one of three treatments: the KROME astrochemistry package (Grassi et al. 2014), which provides a range of different networks for modelling primordial chemistry; the primordial chemistry network implemented in the ENZO adaptive mesh refinement code, described in Bryan et al. (2014), which is a modified and extended version of the network outlined in Abel et al. (1997); or the network introduced in Omukai (2001). We compare our reduced network to each of these treatments below.

3.6.1 The KROME package

The KROME astrochemistry package is a Python-based pre-processing system that converts a simple textual description of an astrochemical network into a set of subroutines for the solution of the chemical rate equations for the species contained in that network. In addition, KROME also contains support for a large number of different heating and cooling processes, allowing the thermal energy equation to be solved along with the chemical rate equations. KROME is still undergoing active development, but in our discussion here we refer to the state of the code at the time of writing;² note that this differs in some respects from the previous version of the package described in Grassi et al. (2014).

The KROME package provides a number of example networks, including several designed for modelling primordial gas. Unfortunately, these come with very little documentation, and so it is not immediately obvious which network is the best choice for which application, or even which (if any) of these networks has been used in studies such as Latif et al. (2014), Van Borm et al. (2014), or Latif et al. (2015) that have been carried out using KROME. However, some investigation allows us to immediately cut down the number of possibilities. We can clearly ignore any of the primordial networks that do not include the photodissociation of H^- or H_2 , since these are crucial processes in the case of the T4 or T5 spectra, respectively. This leaves us with only two

networks to consider: the *react-primordial-photoH2* network and the *react.xrays* network.

The *react-primordial-photoH2* network consists of reactions 1–8, 11, 12, 15, 22, 23, 25 and 26 from our reduced network, along with several additional reactions, largely involving the ionization and recombination of helium and the chemistry of D, D^+ and HD, that our results demonstrate are not important for the determination of J_{crit} . The *react.xrays* network consists of the reactions mentioned above, plus two more from our reduced network, reactions 9 and 18. It also accounts for charge transfer between hydrogen and helium, and includes a more extensive treatment of deuterium chemistry, but once again, our results suggest that these processes are unimportant for determining J_{crit} .

We therefore see that compared to our reduced network, the *react.xrays* network is missing reactions 10, 13–14, 16–17, 19–21 and 24, while the *react-primordial-photoH2* network is missing these plus also reactions 9 and 18. To quantify the effect of omitting these reactions on the determination of J_{crit} , we have rerun our set of six simulations using only the reactions contained in the *react.xrays* network, and determined the value of J_{crit} in each case. Note that when doing so, we use the rate coefficients for each reaction taken from our chemical model, which are not always the same as those adopted by the KROME model. This is because we are interested here only in the effects of omitting some of the reactions that we have determined are important, and not on quantifying the uncertainty introduced into J_{crit} by differences in our choice of rate coefficients. We examine the latter issue at some length in a companion paper (Glover 2015).

The results of our comparison are shown in Table 5. We see that the KROME network systematically underestimates J_{crit} . The discrepancy is worst in run 1, where the error is almost a factor of two, but even in the best case, the error is $\sim 20\%$. We have also carried out a similar comparison using the set of reactions in the *react-primordial-photoH2* network, but find that in this case we recover very similar results. We have investigated the source of this discrepancy and find that almost all of it is accounted for by the omission of reactions 10 and 14 from the KROME model. If we add these two reactions to the set included in the *react.xrays* network, then we can reproduce the values of J_{crit} that we obtain with our minimal model to within $\sim 1\%$.

3.6.2 The ENZO network

The primordial chemistry network implemented in the ENZO code consists of the same subset of the reactions from our minimal model as in the KROME *react.xrays* network, i.e. reactions 1–8, 11, 12, 15, 22, 23, 25 and 26. As in the case of the KROME networks, it also includes a number of reactions involving the ionization and recombination of helium and the chemistry of deuterium that play no role in the determination of J_{crit} . The only difference between the ENZO network and the the KROME *react.xrays* network that is relevant for our present study is that the KROME network accounts for the collisional dissociation of H_2 via dissociative tunneling as well as direct dissociation into the continuum, whereas the ENZO model only includes the latter process.

In Table 5, we compare the values of J_{crit} that we obtain using the ENZO model with those that we obtain using

² Specifically, on January 3rd, 2015, at which time the most recent commit was 53a32c2ab5d53994fe4893676dbfbcf08125c23d

our reduced model. We find that the ENZO model systematically overestimates J_{crit} by between 20% and 50%. Interestingly, the mean difference is smaller than with the KROME model, despite the fact that the ENZO model is less complete than the KROME model. The reason for this is that while the neglect of reactions 10 and 14 in the ENZO model tends to decrease our estimate of J_{crit} , the neglect of dissociative tunneling has the opposite effect, as we have seen already in Section 3.5. Therefore, the two effects cancel to some extent, and so the overall difference with the results of our reduced model is less than we would initially expect.

3.6.3 The Omukai (2001) network

The chemical network adopted by Omukai (2001) in his pioneering study of the effects of a strong extragalactic radiation field on the gravitational collapse of primordial gas includes reactions 1–10, 12, 15, 18, 22 and 26 from our reduced network. It also includes a number of additional reactions such as the three-body recombination of H^+ , or the collisional ionization of electronically excited hydrogen that are unimportant at the densities at which the value of J_{crit} is set, but which play important roles in regulating the ionization state and thermal evolution of the gas at much higher densities. The Omukai (2001) network, which for the sake of brevity we refer to hereafter as the O01 network, or an updated version of it, has subsequently been used in a number of different studies of aspects of the direct collapse model for black hole formation (e.g. Omukai, Schneider & Haiman 2008; Inayoshi & Omukai 2011, 2012; Inyoshi, Omukai & Tasker 2014; Sugimura, Omukai & Inoue 2014).

In Table 5, we compare the results we obtain for J_{crit} when we use the set of reactions contained in the O01 network with the values obtained using our reduced network. In performing this comparison, we have assumed that the O01 network accounts for both the direct collisional dissociation of H_2 and its destruction by dissociative tunneling. This was not the case in the original version of the network, which used a highly outdated treatment of H_2 collisional dissociation taken from Lepp & Shull (1983). More recent studies use an updated treatment based on Martin, Schwarz & Mandy (1996), but do not clarify whether they include only the direct collisional dissociation or also the dissociative tunneling term.

We see from Table 5 that there is very good agreement between the results of our reduced network and those obtained using the O01 network in the case of the simulations performed using the T4 spectrum. In these runs, the maximum difference between the two models is around 2%. The main reason that the O01 model performs much better than the KROME or ENZO models in this case is that it includes the effects of reaction 10, which, as we have already seen, significantly contributes to the ionization state of the gas at the densities where the value of J_{crit} is set.

In the case of the runs performed using the T5 spectrum, however, we see that there is a difference of almost a factor of two between the results from our reduced model and those from the O01 model. This difference is driven almost entirely by the fact that the O01 model does not include reaction 11 from our reduced model, the collisional detachment of H^- by H :



Although this reaction generally occurs more slowly than the associative detachment reaction responsible for forming H_2 from H^- (reaction number 3 in our reduced network), at the temperatures reached in gas with $J_{21} \sim J_{\text{crit}}$, the difference between the two rates is less than an order of magnitude. In the runs with the T4 spectrum, both reactions have rates that are small compared to the photodetachment rate (reaction 7), and hence including reaction 11 in the model makes little difference to the equilibrium H^- abundance or the H_2 formation rate. On the other hand, in runs performed using the T5 spectrum, H^- photodetachment is much less important and so reaction 11 plays a much more important role in regulating the H^- abundance. Its omission from the chemical network leads to one overestimating the H^- abundance and hence overestimating the H_2 formation rate. Consequently, a larger value of J_{21} is required in order to suppress H_2 cooling, and so the resulting values for J_{crit} are systematically larger. We have verified this by re-running the T5 models with a modified version of the O01 network that includes reaction 11. We find that in this case, the difference between the value of J_{crit} that we obtain for the modified O01 model and the one that we obtain for our reduced model is only $\sim 5\%$, with this remaining difference mostly likely being due to the fact that the O01 model does not include the effects of the collisional ionization of H by collisions with He (reaction 14).

4 SUMMARY

In this paper, we have attempted to identify the set of chemical reactions that it is essential to include in any chemical network used to determine J_{crit} , the critical UV flux required to suppress H_2 cooling in atomic cooling halos with $T_{\text{vir}} > 10^4$ K. To do this, we have made use of the reaction-based reduction algorithm developed by Wiebe, Semenov & Henning (2003). This has previously been applied to the study of the chemistry of the local interstellar medium, but to the best of our knowledge, the present paper marks its first use in the study of the chemistry of primordial gas.

Using this reduction technique with a conservative choice of $\epsilon = 10^{-4}$ for the reaction weight below which we do not retain reactions in our reduced network, we find that we can reduce our initial 30 species, ~ 400 reaction network to a reduced network containing only eight chemical species linked by 26 reactions. We have verified that simulations carried out using this reduced network predict essentially identical values of J_{crit} to those carried out using our full network. We have also explored the effect of varying ϵ , and find that we continue to be able to predict J_{crit} accurately as long as $\epsilon \leq 10^{-2}$. Setting $\epsilon = 10^{-2}$ allows us to produce an even smaller “minimal” reduced network, containing the same set of eight chemical species, but now linked by only 18 reactions.

Most of the reactions included in our reduced networks are familiar from previous studies of the chemistry of primordial gas. The main exception is the reaction



This was included in the original investigation by Omukai

(2001) of the effect of strong UV radiation fields on the gravitational collapse of primordial gas, but has been omitted in most subsequent studies. We have investigated the influence of this reaction and show that omitting it leads to a 20-30% reduction in J_{crit} . We also confirm the previous finding of Latif et al. (2014) regarding the importance of accounting for dissociative tunneling when treating H_2 collisional dissociation, and show that omitting this process leads to one overestimating J_{crit} by almost a factor of two.

We have compared the values for J_{crit} that we recover using our reduced network with those that we obtain using several other chemical networks that have previously been adopted in studies of the direct collapse model: the *react_xrays* network from the KROME astrochemistry package, the ENZO primordial chemistry network, and the Omukai (2001) network. In carrying out this comparison we have updated the chemical rate coefficients used in these networks to match those used in the current paper, to allow us to focus on the uncertainties introduced by differences in the set of reactions chosen to construct the different chemical networks. We find that the Omukai (2001) network predicts J_{crit} accurately for the runs with a T4 spectrum, but significantly overestimates it for runs with a T5 spectrum, owing primarily to its neglect of the reaction



We also show that the ENZO network tends to predict values of J_{crit} that are 20–50% larger than those predicted by our reduced model, while the KROME *react_xrays* network predicts values that are 20–50% smaller. The total uncertainty introduced into estimates of J_{crit} given in the literature due to differences between the chemical networks adopted by different studies can therefore approach a factor of three.

To put this number into context, we note that in the regime relevant for the direct collapse model, the probability of an atomic cooling halo being exposed to a local radiation field with a strength $J_{21} > J_{\text{crit}}$ is a strongly decreasing function of J_{crit} (Dijkstra et al. 2014). For example, Inayoshi & Tanaka (2014) show that for $10^3 < J_{\text{crit}} < 10^4$, this probability scales approximately as $P \propto J_{\text{crit}}^{-5}$. A factor of three uncertainty in J_{crit} can therefore potentially correspond to a factor of ~ 200 uncertainty in the cosmological number density of massive black holes formed by direct collapse.

Finally, we stress that this uncertainty can be eliminated from future studies of the direct collapse model simply by ensuring that the chemical network adopted includes the full set of chemical reactions that are important for determining J_{crit} . We therefore recommend that in future work, researchers take care to include, at the very least, all of the reactions making up the minimal reduced model described in Section 3.3.

ACKNOWLEDGEMENTS

The author would like to thank T. Hartwig, S. Khochfar, R. Klessen, and M. Volonteri for useful conversations regarding the physics of black hole formation in the high-redshift Universe. Additional thanks also go to T. Hartwig for his comments on an earlier draft of this paper. Special thanks go to B. Agarwal and B. Smith for several discussions regarding the possible impact of chemical uncertainties on J_{crit} that

inspired the author to carry out the work described here. Financial support for this work was provided by the Deutsche Forschungsgemeinschaft via SFB 881, “The Milky Way System” (sub-projects B1, B2 and B8) and SPP 1573, “Physics of the Interstellar Medium” (grant number GL 668/2-1), and by the European Research Council under the European Community’s Seventh Framework Programme (FP7/2007-2013) via the ERC Advanced Grant STARLIGHT (project number 339177).

REFERENCES

- Abel, T., Anninos, P., Zhang, Y., & Norman, M. L. 1997, *New Astron.*, 2, 181
- Agarwal, B., & Khochfar, S. 2015, *MNRAS*, 446, 160
- Agarwal, B., Khochfar, S., Johnson, J. L., Neistein, E., Dalla Vecchia, C., & Livio, M. 2012, *MNRAS*, 425, 2854
- Ahn, K., Shapiro, P. R., Iliev, I. T., Mellema, G., & Pen, U.-L. 2009, *ApJ*, 695, 1430
- Alvarez, M. A., Wise, J. H., & Abel, T. 2009, *ApJ*, 701, L133
- Barklem, P. S. 2007, *A&A*, 466, 327
- Becerra, F., Greif, T. H., Springel, V., & Hernquist, L. 2015, *MNRAS*, 446, 2380
- Begelman, M. C., Volonteri, M., & Rees, M. J. 2006, *MNRAS*, 370, 289
- Bromm, V., Kudritzki, R. P., & Loeb, A. 2001, *ApJ*, 552, 464
- Bromm, V., & Loeb, A. 2003, *ApJ*, 596, 34
- Bruhns, H., Kreckel, H., Miller, K. A., Urbain, X., & Savin, D. W. 2010, *Phys. Rev. A*, 82, 042708
- Bryan, G. L., et al. 2014, *ApJS*, 211, 19
- Choi, J.-H., Shlosman, I., & Begelman, M. C. 2013, *ApJ*, 774, 149
- Cojazzi, P., Bressan, A., Lucchin, F., Pantano, O., & Chavez, M. 2000, *MNRAS*, 315, L51
- Coppola, C. M., Longo, S., Capitelli, M., Palla, F., & Galli, D. 2011, *ApJS*, 193, 7
- Croft, H., Dickinson, A. S., & Gadea, F. X. 1999, *MNRAS*, 304, 327
- Cybert, R. H. 2004, *Phys. Rev. D*, 70, 023505
- Dijkstra, M., Haiman, Z., Mesinger, A., Wyithe, J. S. B. 2008, *MNRAS*, 391, 1961
- Dijkstra, M., Ferrara, A., & Mesinger, A. 2014, *MNRAS*, 442, 2036
- Draine, B. T., & Bertoldi, F. 1996, *ApJ*, 468, 269
- Draine, B. T., Roberge, W. G., & Dalgarno, A. 1983, *ApJ*, 264, 485
- Drawin, H.-W., 1969, *Zeit. Phys.* 225, 470
- Dunn, G. H., 1968, *Phys. Rev.*, 172, 1
- Forrey, R. C. 2013a, *ApJ*, 773, L25
- Forrey, R. C. 2013b, *Phys. Rev. A*, 88, 052709
- Fussen, D., & Kubach, C. 1986, *J. Phys. B*, 19, L31
- Galli, D., & Palla, F., 1998, *A&A*, 335, 403
- Gealy, M. W., & van Zyl, B. 1987, *Phys. Rev. A*, 36, 3100
- Gerlich, D., 1990, *J. Chem. Phys.*, 92, 2377
- Gerlich, D., Jusko, P., Roučka, Š., Zymak, I., Plašil, R., & Glořík, J. 2012, *ApJ*, 749, 22
- Glover, S. 2008, in “First Stars III”, eds. B. W. O’Shea, A. Heger, & T. Abel, *AIP Conf. Proc.* Volume 990, p. 25

- Glover, S. C. O., 2015, MNRAS, submitted; arXiv:1504.00514
- Glover, S. C. O., & Abel, T., 2008, MNRAS, 388, 1627
- Glover, S. C. O., & Savin, D. W. 2009, MNRAS, 393, 911
- Glover, S. C., Savin, D. W., & Jappsen, A.-K. 2006, ApJ, 640, 553
- Grassi, T., Bovino, S., Schleicher, D. R. G., Prieto, J., Seifried, D., Simoncini, E., & Gianturco, F. A. 2014, MNRAS, 439, 2386
- Greif, T. H., & Bromm, V. 2006, MNRAS, 373, 128
- Greif, T. H., 2015, Comp. Astro. Cosmol., 2, 3
- Haiman, Z., Abel, T., & Rees, M. J. 2000, ApJ, 534, 11
- Haiman, Z., 2013, in *The First Galaxies*, eds. T. Wiklund, B. Mobasher, & V. Bromm, Astrophys. Space Sci. Library, Volume 396, (Berlin: Springer), 293
- Hollenbach, D., & McKee, C. F. 1979, ApJS, 41, 555
- Hollenbach, D., & McKee, C. F. 1989, ApJ, 342, 306
- Honvault, P., Jorfi, M., González-Lezana, T., Faure, A., & Pagani, L. 2011, Phys. Rev. Lett., 107, 023201
- Honvault, P., Jorfi, M., González-Lezana, T., Faure, A., & Pagani, L. 2012, Phys. Rev. Lett., 108, 109903
- Kreckel, H., Bruhns, H., Čížek, M., Glover, S. C. O., Miller, K. A., Urbain, X., & Savin, D. W. 2010, Science, 329, 69
- Krzić, P. S. 2002, Phys. Rev. A, 66, 042717
- Krzić, P. S., & Janev, R. K. 2003, Phys. Rev. A, 67, 022708
- Kunc, J. A., & Soon, W. H. 1991, J. Chem. Phys., 95, 5738
- Inayoshi, K., & Omukai, K. 2011, MNRAS, 416, 2748
- Inayoshi, K., & Omukai, K. 2012, MNRAS, 422, 2539
- Inayoshi, K., Omukai, K., & Tasker, E. 2014, MNRAS, 445, L109
- Inayoshi, K., & Tanaka, T. L. 2014, MNRAS, in press; arXiv:1411.2590
- Latif, M. A., Schleicher, D. R. G., Schmidt, W., & Niemeyer, J. C. 2013a, MNRAS, 436, 2989
- Latif, M. A., Schleicher, D. R. G., Schmidt, W., & Niemeyer, J. C. 2013b, MNRAS, 433, 1607
- Latif, M. A., Bovino, S., Van Borm, C., Grassi, T., Schleicher, D. R. G., & Spaans, M. 2014, MNRAS, 443, 1979
- Latif, M. A., Bovino, S., Grassi, T., Schleicher, D. R. G., & Spaans, M. 2015, MNRAS, 446, 3163
- Lenzuni, P., Chernoff, D. F., & Salpeter, E. E. 1991, ApJS, 76, 759
- Lepp, S., & Shull, J. M. 1983, ApJ, 270, 578
- Martin, P. G., Schwarz, D. H., & Mandy, M. E. 1996, ApJ, 461, 265
- Martinez, O., Yang, Z., Betts, N. B., Snow, T. P., & Bierbaum, V. M. 2009, ApJ, 705, L172
- Miller, K. A., Bruhns, H., Eliášek, J., Čížek, M., Kreckel, H., Urbain, X., & Savin, D. W. 2011, Phys. Rev. A, 84, 052709
- Miller, K. A., Bruhns, H., Čížek, M., Eliášek, J., Cabrera-Trujillo, R., Kreckel, H., O'Connor, A. P., Urbain, X., & Savin, D. W. 2012, Phys. Rev. A, 86, 032714
- Mortlock, D. J., et al., 2011, Nature, 474, 616
- Omukai, K., 2001, ApJ, 546, 635
- Omukai, K., Schneider, R., & Haiman, Z. 2008, ApJ, 686, 801
- Ramaker, D. E., & Peek, J. M. 1976, Phys. Rev. A, 13, 58
- Regan, J. A., & Haehnelt, M. G. 2009, MNRAS, 396, 343
- Regan, J. A., Johansson, P. H., & Haehnelt, M. G. 2014, MNRAS, 439, 1160
- Savin, D. W., Krstić, P. S., Haiman, Z., & Stancil, P. C. 2004a, ApJ, 606, L167
- Savin, D. W., Krstić, P. S., Haiman, Z., & Stancil, P. C. 2004b, ApJ, 607, L147
- Schleicher, D. R. G., Spaans, M., & Glover, S. C. O. 2010, ApJ, 712, L69
- Schneider, I. F., Dulieu, O., Giusti-Suzor, A., & Roueff, E. 1994, ApJ, 424, 983
- Schneider, I. F., Dulieu, O., Giusti-Suzor, A., & Roueff, E. 1997, ApJ, 486, 580
- Shang, C., Bryan, G. L., & Haiman, Z. 2010, MNRAS, 402, 1249
- Shapiro, P. R., & Kang, H. 1987, ApJ, 318, 32
- Soon, W. H. 1992, ApJ, 394, 717
- Stancil, P. C. 1994, ApJ, 430, 360
- Stancil, P. C., Babb, J. F., & Dalgarno, A. 1993, ApJ, 414, 672
- Stenrup, M., Larson, A., & Elander, N. 2009, Phys. Rev. A, 79, 012713
- Sugimura, K., Omukai, K., & Inoue, A. K. 2014, MNRAS, 445, 544
- Takagi, T. 2002, Phys. Scripta, T96, 52
- Tanaka, T., & Haiman, Z. 2009, ApJ, 696, 1798
- Türk, M. J., Clark, P., Glover, S. C. O., Greif, T. H., Abel, T., Klessen, R., & Bromm, V. 2011, ApJ, 726, 55
- Urbain, X., Lécointre, J., Mezdari, F., Miller, K. A., & Savin, D. W. 2012, J. Phys. Conf. Ser., 388, 092004
- Van Borm, C., Bovino, S., Latif, M. A., Schleicher, D. R. G., Spaans, M., & Grassi, T. 2014, A&A, 572, 22
- Van Zyl, B., Le, T. Q., & Amme, R. C., 1981, J. Chem. Phys., 74, 314
- Visbal, E., Haiman, Z., & Bryan, G. L. 2014, MNRAS, 442, L100
- Volonteri, M., 2010, A&A Rev. 18, 279
- Wiebe, D., Semenov, D., & Henning, Th. 2003, A&A, 399, 197
- Wolcott-Green, J., & Haiman, Z. 2011, MNRAS, 412, 2603
- Wolcott-Green, J., Haiman, Z., & Bryan, G. L. 2011, MNRAS, 418, 838
- Yoon, J.-S., Song, M.-Y., Han, J.-M., Hwang, S. H., Chang, W.-S., Lee, B., & Itikawa, Y. 2008, J. Phys. Chem. Ref. Data, 37, 913

APPENDIX A: REVISIONS TO THE THERMAL MODEL

We have improved on the thermal model introduced in Glover & Abel (2008) and Glover & Savin (2009) by updating the rates of two of the cooling processes in an effort to use the most up-to-date data available. Details of our changes are given below.

A1 Updated cooling rates

A1.1 Collisional excitation of H_2 by electrons

The cooling rate due to collisions between H_2 molecules and free electrons that we used in Glover & Savin (2009) was taken from Glover & Abel (2008) and was based on rather old data from Draine, Roberge & Dalgarno (1983). We have now updated our treatment of this process and use a rate

based on data from the recent compilation of Yoon et al. (2008). The resulting cooling rate is well fit by the expression

$$\begin{aligned} \log \Lambda_{\text{H}_2, \text{e}} = & -21.928796 + 16.815730 \log(T_3) \\ & + 96.743155 \log(T_3)^2 \\ & + 343.19180 \log(T_3)^3 \\ & + 734.71651 \log(T_3)^4 \\ & + 983.67576 \log(T_3)^5 \\ & + 801.81247 \log(T_3)^6 \\ & + 364.14446 \log(T_3)^7 \\ & + 70.609154 \log(T_3)^8, \end{aligned} \quad (\text{A1})$$

at temperatures $100 < T < 500$ K, and by

$$\begin{aligned} \log \Lambda_{\text{H}_2, \text{e}} = & -22.921189 + 1.6802758 \log(T_3) \\ & + 0.93310622 \log(T_3)^2 \\ & + 4.0406627 \log(T_3)^3 \\ & - 4.7274036 \log(T_3)^4 \\ & - 8.8077017 \log(T_3)^5 \\ & + 8.9167183 \log(T_3)^6 \\ & + 6.4380698 \log(T_3)^7 \\ & - 6.3701156 \log(T_3)^8, \end{aligned} \quad (\text{A2})$$

at temperatures $500 < T < 10^4$ K, where $T_3 = T/1000$ K. These fits are accurate to within 5% over the quoted temperature range. This revised treatment yields less cooling at all temperatures than the rate given in Glover & Abel (2008), with the effect being particularly pronounced at temperatures around 1000 K. However, the effect on the total H_2 cooling rate is less significant, since $\text{H}_2\text{-H}^+$ collisions lead to substantially more cooling than $\text{H}_2\text{-e}^-$ collisions in gas where $n_{\text{H}^+} \simeq n_{\text{e}}$.

A1.2 Collisional excitation of H_2 by protons

We have also updated our treatment of the cooling rate due to collisions between H_2 molecules and protons. The treatment in Glover & Savin (2009) was based on Glover & Abel (2008) and made use of data from Gerlich (1990) and Krstić (2002). Our new treatment makes use of the excitation rates recently calculated by Honvault et al. (2011, 2012) for the transitions for which these are available, supplementing them with data from Gerlich (1990) and Krstić (2002) for those transitions for which newer data is not available. The resulting cooling rate is well fit by the expression

$$\begin{aligned} \log \Lambda_{\text{H}_2, \text{H}^+} = & -22.089523 + 1.5714711 \log(T_3) \\ & + 0.015391166 \log(T_3)^2 \\ & - 0.23619985 \log(T_3)^3 \\ & - 0.51002221 \log(T_3)^4 \\ & + 0.32168730 \log(T_3)^5, \end{aligned} \quad (\text{A3})$$

for temperatures in the range $10 < T < 10^4$ K. Again, the revised treatment yields less cooling at all temperatures than the rate given in Glover & Abel (2008). In conditions where $\text{H}_2\text{-H}^+$ collisions make the dominant contribution to the H_2 cooling function, the total H_2 cooling rate can be as much as a factor of two smaller.

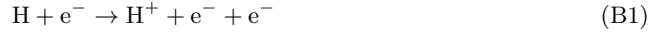
APPENDIX B: REVISIONS TO THE CHEMICAL MODEL

We have improved on the chemical model introduced in Glover & Savin (2009) by including three new reactions and updating the reaction rates used for a further eight reactions. Details of our changes are given below.

B1 New reactions

B1.1 Collisional ionization of atomic hydrogen

Because the rate at which electrons bring about the collisional ionization of atomic hydrogen



is substantially faster than the ionization rate due to H-H collisions



the latter process has been omitted from most chemical models of primordial gas. However, it can actually dominate if the fractional ionization of the gas falls below $x \sim 10^{-4}$, or if there is a substantial population of H atoms in excited electronic states (Omukai 2001). We therefore include this process in our revised chemical model, using the following rate coefficient (Lenzuni, Chernoff & Salpeter 1991; Omukai 2001).

$$k_{\text{ci, H}} = 1.2 \times 10^{-17} T^{1.2} \exp\left(\frac{-157800}{T}\right) \text{ cm}^3 \text{ s}^{-1}. \quad (\text{B3})$$

This rate coefficient is based on the experimental cross-sections measured by Gealy & van Zyl (1987), and assumes that both hydrogen atoms are in their ground state. As we discuss in more detail in Paper II, a number of other versions of the rate coefficient for this reaction can be found in the literature (Drawin 1969; Hollenbach & McKee 1979, 1989; Kunc & Soon 1991; Soon 1992; Barklem 2007). These expressions differ by large amounts at the temperatures relevant for this study and it is unclear which expression gives the best description of the actual behaviour of this reaction. In this paper, we have chosen to use the version of the rate coefficient given in Lenzuni, Chernoff & Salpeter (1991) for consistency with the earlier study of Omukai (2001), but in Paper II we explore the sensitivity of J_{crit} to this choice.

We also include the collisional ionization of atomic hydrogen by collisions with neutral helium



We use the rate coefficient computed by Lenzuni, Chernoff & Salpeter (1991) using cross-sections from Van Zyl, Le & Amme (1981):

$$k_{\text{ci, He}} = 1.75 \times 10^{-17} T^{1.3} \exp\left(\frac{-157800}{T}\right) \text{ cm}^3 \text{ s}^{-1}. \quad (\text{B5})$$

Again, this expression assumes that all of the hydrogen atoms are in their ground state.

In practice, trapping of Lyman- α photons in the collapsing gas owing to the high optical depth in the Lyman- α line leads to the existence of a non-zero population of hydrogen atoms in excited electronic states (see e.g. Omukai 2001; Schleicher, Spaans & Glover 2010). However, at the densities of interest in this study, only a very small fraction (of order

10^{-10} or less) of the total number of hydrogen atoms are found in these states (Schleicher, Spaans & Glover 2010), and so there is no need to account in the chemical model for the effects of collisional ionization out of these states.

B1.2 Collisional dissociation of H_2^+ by atomic hydrogen

We now account for the destruction of H_2^+ by the reaction



The rate at which this reaction proceeds depends on the internal excitation of the H_2^+ molecular ion. At low densities, it is safe to assume that all of the ions are in the vibrational ground state. In this limit, we adopt the following rate coefficient for this reaction

$$k_{cd,0} = 1.54 \times 10^{-12} T^{0.45} \exp\left(\frac{-31000}{T}\right) \text{ cm}^3 \text{ s}^{-1}, \quad (B7)$$

which we have derived based on the cross-sections presented in Krstić & Janev (2003). At high densities, on the other hand, the vibrational level populations of the H_2^+ ion approach their local thermodynamic equilibrium (LTE) values. In this limit, we use the LTE rate for this reaction derived by Coppola et al. (2011), which was again based on the Krstić & Janev (2003) cross-sections. At intermediate densities, we interpolate between these two limiting cases by adopting a rate coefficient of the form

$$k_{cd} = k_{cd,LTE} \left(\frac{k_{cd,0}}{k_{cd,LTE}} \right)^\alpha, \quad (B8)$$

where $k_{cd,LTE}$ is the rate coefficient in the LTE limit, $\alpha = (1 + n/n_{crit})^{-1}$, and n_{crit} is the critical density for H_2^+ (i.e. the density at which the effects of collisional de-excitation and radiative de-excitation become comparable).

As explained in Glover & Savin (2009), in primordial gas the dominant contributions to the collisional excitation or de-excitation of H_2^+ come from collisions with atomic hydrogen or with electrons. When collisions with H atoms dominate, we can estimate the critical density by taking the ratio of the cooling rates due to H_2^+ in the LTE and low density limits, using the expressions for these given in Glover & Savin (2009). The resulting values are reasonably well approximated by the expression

$$n_{crit,H} \simeq 400 T_4^{-1} \text{ cm}^{-3}, \quad (B9)$$

where $T_4 = T/10^4 \text{ K}$. A similar procedure applied to collisions with electrons yields a critical density of electrons that does not vary significantly with temperature, and that is roughly an order of magnitude smaller than $n_{crit,H}$,

$$n_{crit,e} \simeq 50 \text{ cm}^{-3}. \quad (B10)$$

We combine the contributions from atomic hydrogen and free electrons by taking a weighted harmonic average, yielding

$$n_{crit} = \left(\frac{x_H}{n_{crit,H}} + \frac{x_e}{n_{crit,e}} \right)^{-1}. \quad (B11)$$

Although this is a somewhat crude approximation, it is sufficient for our purposes, since J_{crit} is not very sensitive to the treatment adopted for H_2^+ excitation (see Section 3.4).

B2 Updated reaction rates

Since the publication of Glover & Savin (2009), new experimental and/or theoretical data has become available for a number of different reactions. We have therefore updated the rates adopted for several of the included reactions, as detailed below.

B2.1 Associative detachment of H^- with H

The rate coefficient for the reaction



was recently measured by Kreckel et al. (2010) for temperatures in the range $1 < T < 10^4 \text{ K}$ using a merged-beam approach (see also Bruhns et al. 2010; Miller et al. 2011). The estimated systematic error in their measurements is around 25%. Their results disagree with the flowing afterglow results of Martinez et al. (2009) at 300 K by a factor of two, for reasons which remain uncertain, but agree well with the measurements made by Gerlich et al. (2012) at temperatures $10 < T < 150 \text{ K}$ using an ion trap. We therefore adopt the rate coefficient of Kreckel et al. (2010) for this reaction. We also adopt the same rate coefficients for the isotopic variants of this reaction (i.e. reactions where one or both H atoms are replaced by D atoms), following Miller et al. (2012), who found that there is no significant isotope effect in the cross-section for this reaction.

B2.2 Mutual neutralization of H^- with H^+

Until relatively recently, the rate of the mutual neutralization reaction



at low temperatures was quite unclear. Glover, Savin & Jappsen (2006) surveyed the range of rates given for this reaction in the astrophysical literature as of 2006, and showed that there was almost an order of magnitude scatter in the values. Fortunately, the last few years have seen a significant improvement in this area. New theoretical (Stenrup, Larson & Elander 2009) and experimental (Urbain et al. 2012) determinations of the rate coefficient yield values that are in good agreement with the ones derived by Croft, Dickinson & Gadea (1999) from the cross-sections of Fussen & Kubach (1986). We therefore adopt the Croft, Dickinson & Gadea (1999) rate coefficient for use in our study.

B2.3 Dissociative recombination of H_2^+

The rate coefficient used in Glover & Savin (2009) for the reaction



was a fit made by Abel et al. (1997) to the data of Schneider et al. (1994, 1997). It assumes that the H_2^+ molecular ions are in their vibrational ground state. However, this is true only at low densities. At high densities, the H_2^+ level populations tend towards their local thermodynamic equilibrium (LTE) values, and the resulting dissociative recombination rate can be significantly larger (see e.g. the comparison of low density and LTE rates in Figure 9 of Coppola et al.

2011). To account for this, we use a density dependent rate coefficient of the form

$$k_{\text{dr}} = k_{\text{dr,LTE}} \left(\frac{k_{\text{dr},0}}{k_{\text{dr,LTE}}} \right)^\alpha, \quad (\text{B15})$$

where $k_{\text{dr},0}$ is the rate coefficient in the low density limit (taken as before from Abel et al. 1997), $k_{\text{dr,LTE}}$ is the rate coefficient in the LTE limit (taken from Coppola et al. 2011, based on data from Takagi 2002), $\alpha = (1 + n/n_{\text{crit}})^{-1}$, and n_{crit} is the critical density for H_2^+ , calculated as outlined in Section B1.2 above.

B2.4 Collisional dissociation of H_2 by H

We now use the fitting formulae given in Martin, Schwarz & Mandy (1996) to determine the rate coefficient for the reaction



in place of the combination of data from several sources used in Glover & Savin (2009). Importantly, we include the contribution to the total H_2 dissociation rate due to excitation to a quasi-bound state followed by dissociative tunneling to an unbound state (γ_{dt} in the notation of Martin, Schwarz & Mandy 1996). At low temperatures ($T < 4500$ K in the low density limit), this effect is more important than direct collisional dissociation and it is important to account for it if one wants to determine J_{crit} accurately (see Latif et al. 2014 or Section 3.5 of the present paper).

B2.5 Charge transfer from H^+ to H_2

Glover & Savin (2009) adopted a rate coefficient for the reaction



that was taken from Savin et al. (2004a,b) and that assumes that all of the H_2 molecules are in their vibrational ground state. However, in the LTE limit, the actual rate can be as much as an order of magnitude larger (Coppola et al. 2011). In the present study, we therefore adopt a density-dependent rate coefficient of the form

$$k_{\text{ct}} = k_{\text{ct,LTE}} \left(\frac{k_{\text{ct},0}}{k_{\text{ct,LTE}}} \right)^\alpha, \quad (\text{B18})$$

where $k_{\text{ct},0}$ is the rate coefficient in the low density limit (taken from Savin et al. 2004a,b), $k_{\text{ct,LTE}}$ is the rate coefficient in the LTE limit (taken from Coppola et al. 2011), $\alpha = (1 + n/n_{\text{crit}})^{-1}$, and n_{crit} is the H_2 critical density. We conservatively assume that the latter has the same value here as for collisions between H_2 and H .

B2.6 Three-body formation of H_2

A large variety of different rate coefficients have been given in the astrophysical literature for the reaction



as summarized in Glover (2008) and Turk et al. (2011). Typically, these values were derived by taking the

experimentally-measured rate for the inverse process (collisional dissociation of H_2 by H) and then applying the principle of detailed balance. In general, the resulting rate coefficients agree fairly well at high temperatures (where the collisional dissociation rate can be easily measured), but disagree substantially at low temperatures, owing in large part to the errors introduced by extrapolating the collisional dissociation rates outside of the measured temperature range.

This unsatisfactory state of affairs was recently addressed by Forrey (2013a,b). He computed a rate coefficient for this reaction using a new technique that does not rely on detailed balance and that hence should be far more reliable at low gas temperatures. The resulting rate coefficient is well fit by the simple expression (Forrey 2013a)

$$k_{3b} = 6 \times 10^{-32} T^{-1/4} + 2 \times 10^{-31} T^{-1/2} \text{ cm}^6 \text{ s}^{-1}, \quad (\text{B20})$$

and we use this value in all of our calculations.

B2.7 Photodissociation of H_2^+

The rate adopted by Glover & Savin (2009) for the process



assumed at T5 spectrum and also that all of the H_2^+ molecular ions were in their vibrational ground state. The latter assumption is reasonable at the redshifts of interest in this study provided that the gas density is significantly lower than the H_2^+ critical density. However, as $n \rightarrow n_{\text{crit}}$, it becomes important to account for the effects of vibrational excitation, as this can potentially have a large influence on the photodissociation rate (Galli & Palla 1998).

In our present study, we have therefore calculated H_2^+ photodissociation rates for the limiting cases where all of the molecular ions are in the $v = 0$ state and where the vibrational level populations have their LTE values. In the $v = 0$ case, we use the expression

$$k_{\text{pd,H}_2^+,v=0} = 2.0 \times 10^{11} T_{\text{rad}}^{1.59} \exp\left(-\frac{82000}{T_{\text{rad}}}\right) \text{ s}^{-1} \quad (\text{B22})$$

given by Galli & Palla (1998), based on data from Dunn (1968), to compute the photodissociation rate for a blackbody spectrum and then rescale both the strength of the spectrum and the size of the rate by the same amount so that the resulting specific intensity at the Lyman limit is given by $10^{-21} \text{ ergs}^{-1} \text{ cm}^{-2} \text{ Hz}^{-1} \text{ sr}^{-1}$. For a T4 spectrum, this procedure yields a photodissociation rate given by

$$k_{\text{pd,H}_2^+,v=0} = 1.74 \times 10^{-10} J_{21} \text{ s}^{-1}, \quad (\text{B23})$$

while for a T5 spectrum we have

$$k_{\text{pd,H}_2^+,v=0} = 5.77 \times 10^{-12} J_{21} \text{ s}^{-1}. \quad (\text{B24})$$

In the LTE case, the H_2^+ photodissociation rate depends on the gas temperature, which we cannot assume is the same as the radiation temperature. We therefore cannot use the formula given in Galli & Palla (1998), which does assume that $T_{\text{gas}} = T_{\text{rad}}$, but instead compute the required rates using the cross-sections given in Stancil (1994). These are valid for temperatures in the range $3150 < T < 25200$ K. We find that for temperatures in this range, the H_2^+ photodissociation rate for a T4 spectrum is well-fit in the temperature range $3150 < T < 9000$ K by the following expression

$$k_{\text{pd},\text{H}_2^+,\text{LTE}} = 3.45 \times 10^{-8} \exp\left(-\frac{8500}{T}\right) J_{21} \text{ s}^{-1}, \quad (\text{B25})$$

and at temperatures $9000 < T < 25200$ K by the expression

$$k_{\text{pd},\text{H}_2^+,\text{LTE}} = 2.5 \times 10^{-7} T^{-0.22} \exp\left(-\frac{8500}{T}\right) J_{21} \text{ s}^{-1}. \quad (\text{B26})$$

Within the range of temperatures quoted above, the fitting error of these expressions is no more than 10%. At temperatures $T < 3150$ K, we extrapolate using Equation B25 until we reach the rate given by Equation B23, since the $v = 0$ rate is also the appropriate low T limit of the LTE rate. At temperatures $T > 25200$ K, we could in principle again extrapolate using Equation B26, but in practice, the gas in our models never reaches these temperatures.

For the T5 spectrum, we use a similar procedure. In this case, the LTE rate is well-fit over the whole temperature range $3150 < T < 25200$ K by the expression

$$k_{\text{pd},\text{H}_2^+,\text{LTE}} = 2.2 \times 10^{-11} T^{-0.22} J_{21} \text{ s}^{-1}. \quad (\text{B27})$$

As before, at temperatures $T < 3150$ K, we extrapolate the rate coefficient using the same expression until we reach the value given by Equation B24.

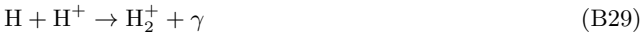
Finally, in our numerical models we smoothly interpolate between the two limiting cases using the following expression:

$$k_{\text{pd},\text{H}_2^+} = k_{\text{pd},\text{H}_2^+,\text{LTE}} \left(\frac{k_{\text{pd},\text{H}_2^+,v=0}}{k_{\text{pd},\text{H}_2^+,\text{LTE}}} \right)^\alpha, \quad (\text{B28})$$

where $\alpha = (1 + n/n_{\text{crit}})^{-1}$, and n_{crit} is the critical density of H_2^+ , computed as described in Section B1.2 above.

B2.8 Formation of H_2^+ by radiative association

Rate coefficients for the reaction



have been computed by both Ramaker & Peek (1976) and Stancil, Babb & Dalgarno (1993), and agree to within 3%. However, the analytical fits to this data used in most current models of primordial chemistry are rather less accurate. Many models use the fit introduced by Shapiro & Kang (1987), which has the form

$$k_{\text{ra},\text{H}_2^+} = 1.85 \times 10^{-23} T^{1.8} \text{ cm}^3 \text{ s}^{-1} \quad (\text{B30})$$

for $T < 6700$ K and

$$k_{\text{ra},\text{H}_2^+} = 5.81 \times 10^{-16} \left(\frac{T}{56200} \right)^{\eta(T)} \text{ cm}^3 \text{ s}^{-1} \quad (\text{B31})$$

for $T > 6700$ K, where $\eta(T) = -0.6657 \log(T/56200)$. On the other hand, the Glover & Savin (2009) model uses instead the fit given in Galli & Palla (1998)

$$k_{\text{ra},\text{H}_2^+} = \text{dex} \left[-19.38 - 1.523 \log T + 1.118 (\log T)^2 - 0.1269 (\log T)^3 \right] \text{ cm}^3 \text{ s}^{-1}. \quad (\text{B32})$$

Although both of these analytical fits are based on the Ramaker & Peek (1976) data, they differ from each other, and from the rates tabulated in by Ramaker & Peek, by as much as 30%. For this reason, in our current study we do not use either of these prescriptions. Instead, we use the analytical

fit given in the recent paper by Latif et al. (2015), and based on the work of Coppola et al. (2011)

$$k_{\text{ra},\text{H}_2^+} = \text{dex} \left[-18.20 - 3.194 \log T + 1.786 (\log T)^2 - 0.2072 (\log T)^3 \right] \text{ cm}^3 \text{ s}^{-1}. \quad (\text{B33})$$

The fit gives values for the rate coefficients that agree with those tabulated by Ramaker & Peek (1976) to within around 5-6%. Moreover, at the temperatures most relevant in this study, $T \sim 4000$ – 8000 K, the agreement is even better, with the fit differing from the tabulated values by no more than 1-2%.